15th IFK
Proc. of the 15th International Fluid Power Conference <Symposium/Conference>
<DOI>

EHAs in mobile machinery: Experimental validation of a high-speed EHA with recuperation and load-holding capability

Felix Figge, Katharina Schmitz

RWTH Aachen University, Institute for Fluid Power Drives and Systems (ifas)

felix.figge@ifas.rwth-aachen.de

Abstract.

The electrification of mobile machinery is advancing, with more machines now featuring battery-electric power sources. However, this shift often results in reduced energy availability and shorter operating hours before recharging is needed. This has led to increased interest in efficient systems driven by the need for energy conservation and emission reduction, alongside relevant legislation.

Traditional hydraulic systems in mobile machinery have demonstrated poor energy efficiency [1,2], highlighting significant improvement potential. Decentralized electro-hydraulic actuators (EHAs) consume less energy than conventional load-sensing systems [2,3], yet their adoption remains limited, possible due to higher costs, unwanted oscillations from mode switching, and increased spatial requirements.

To address these issues, an EHA with a high-speed internal gear unit and electronically controlled valves was developed. The design enables energy recuperation and load-holding while keeping costs low by using a single prime mover and hydraulic unit. High operational speeds reduce installation volume, and the used electronic valves facilitate a control strategy that synchronizes motor speed and valve positions as best as possible. Active hysteresis control and throttling minimize cylinder velocity deviations.

This paper presents the functional model of the EHA and its experimental validation through a hardware-in-the-loop (HiL) test rig. Predefined synthetic test cases are utilized to analyze quadrant switching, demonstrating effective velocity tracking, with minor deviations during transitions. Additionally, measured load cycles of an excavator indicate sufficient position tracking and high efficiency, especially when implemented on the boom.

Keywords. EHA, 4Q-operation, electrification, active throttling, hysteresis control

1. Introduction & State of the Art

Substituting the combustion engine is arguably the most significant change in mobile hydraulics in recent decades. Historically, most machines have utilized a centralized hydraulic pressure supply, with power distributed through fluid lines and valves to various actuators. While this approach is cost-effective in terms of initial component cost, it is relatively inefficient in terms of energy consumption. The different pressure levels required by the actuators during operation, combined with a single pressure supply, inherently result in significant throttle losses. This contradicts the common understanding of the need to conserve energy and reduce emissions, particularly in the context of the lower energy density and higher costs associated with alternative energy sources. Therefore, the hydraulic system of mobile machinery must become more efficient and sustainable.

Decentralized electro-hydraulic actuators (EHAs) can significantly reduce energy losses by using a dedicated pump for each actuator, eliminating throttling losses between varying pressure levels. However, despite their increasing use in stationary industrial applications, EHAs have not yet gained traction in mobile machinery. This is mostlikely due to higher initial component costs, increased installation space requirements, reduced damping linked to lower system losses, and more complex control software. The additional prime mover and hydraulic unit contribute significantly to the higher costs, while the larger footprint complicates integration into existing machines. Latter can be partly counteracted by an increase in rotational speed, reducing the volume of the electric motor and the displacement volume of the pump. Some research even attempted to increase the motor speed further by use of an intermediate gear [4]–[8].
Consequently, this research aims to develop a high-speed closed-circuit EHA for mobile machinery, featuring recuperation and load-holding capabilities, while also establishing the foundation for the necessary software implementation [9]–[12].

Closed-circuit electro-hydraulic actuators (EHAs) with a single pump may display undesirable behavior during quadrant transitions, such as oscillations and frequent mode switches. Pressure feedback is often used to increase the overall damping of the system [13,14], which is typically too low for optimal performance. Williamson and Ivantysynova [15] developed a predictive observer for feed-forward control of pump displacement in skid-steer applications, addressing excessive phase lag that hampers feedback control during mode-switching oscillations. They identified the interaction between moving mass and compressible fluid as a key issue, comparing it to a mass-spring-damper system [13,14].
To mitigate oscillations and prevent mode switches, increasing system damping through pressure feedback is recommended. Michel calculated maximum allowable acceleration to further prevent mode switches [14]. Wang et al. [16] employed electrically actuated proportional valves with a control algorithm to introduce leakage under critical conditions, selectively enhancing damping at low loads. Çalışkan et al. proposed a mechanical solution using an underlapped shuttle valve instead of electrical component [17]. Imam et al. introduced the ‘limited throttling valve’ designed to restrict cylinder outflow at low loads near critical operating conditions, demonstrating no oscillations in simulations [18,19]. This valve is designed to restrict cylinder flow only at low loads near critical operating conditions. Their simulation results show no oscillations under any operating conditions. They also demonstrate that applying different charge pressures to both sides of the cylinder can reduce the critical zone and oscillation amplitudes [19]. Costa and Sepehri [20] introduced a new four-quadrant definition based on cylinder load pressure rather than pressure difference over the pump. They concluded that this was the primary reason for the poor performance of previous circuits and introduced a new circuit that implements their quadrant definition.

However, Gøytil et al. [21] showed that the proposed circuit can still experience unwanted mode switches under certain conditions due to dynamic factors. They recommend using a software-based observer to calculate a modified force estimate, which determines valve states and mitigates these switches. This approach excludes forces from valve switching and acceleration but requires a minimum accumulator pressure of 30 bar to prevent cavitation, which may not be feasible for all circuits. Kärnell and Ericson [22] investigated hysteresis control to prevent unwanted mode switches. They concluded that pressures should be sensed so that the difference remains unchanged after a mode switch. Nevertheless, switches can still occur, but active hysteresis control reduces the risk if the reservoir pressure is sufficient.

The control approach discussed in this paper, first introduced in [9], utilizes the cylinder load pressure definition from Equation 1.1 [17,20] and implements active throttling [19,22] to enable complete coverage of the four quadrants for excavators. To minimize mode switches caused by minor pressure fluctuations, active hysteresis is incorporated [22]. Additionally, the approach minimizes cylinder velocity spikes during quadrant transitions by decoupling the cylinder from the pump using the load-holding valves.

$$p_{load} = p_{pist} - \alpha \cdot p_{rod} \tag{1.1}$$

The paper is structured as follows: Section 2 presents the circuit layout and functional model of the EHA, along with a summary of the control scheme. Section 3 introduces the experimental validation setup, and Section 4 presents the results and discussion.

2. Design & Control of EHA

In this section, first, the design of the developed EHA and the assembled functional model are introduced. Secondly, the hardware-in-the-loop test rig used for validation of the EHA in all quadrants (Q1 to Q4) under a wide range of operational conditions is presented.

2.1. EHA Design

The EHA design under investigation, introduced in [9], is specifically tailored for mobile machinery integration, particularly excavators. Key requirements included minimizing initial costs, achieving a wide range of operating conditions with high efficiency, and enabling complete stoppage of the prime movers. As shown in the circuit layout at the top of Figure 2.1, the design features only a single prime mover, one pump, and a standard differential cylinder. The accumulator stores the differential cylinder volume by switching the 'differential' valves ($Diff_{pist}$ and $Diff_{rod}$). Load-holding capability is realized by two electric actuated proportional valves denoted LH_{pist} and LH_{rod}. The use of proportional valves is required to allow throttling of the cylinder outflow and thereby expanding the range of Q1 and Q3 operation, as detailed in [9]. Otherwise, throttling losses from the load-holding valves prevent high velocities in combinations with low assistive loads, compromising full four-quadrant operation essential for mobile machinery's variable working conditions.

The functional model of the EHA is shown at the bottom of Figure 2.1, with key components labeled. A PMSM electric motor was chosen for its low operating voltage (48 V) and maximum rotational speed of 7,200 rpm, constrained by inverter dual-use regulations. Due to the limited availability of motors that meet these criteria, the motor is oversized with a continuous power rating of approximately 10 kW. In contrast, the peak power output during

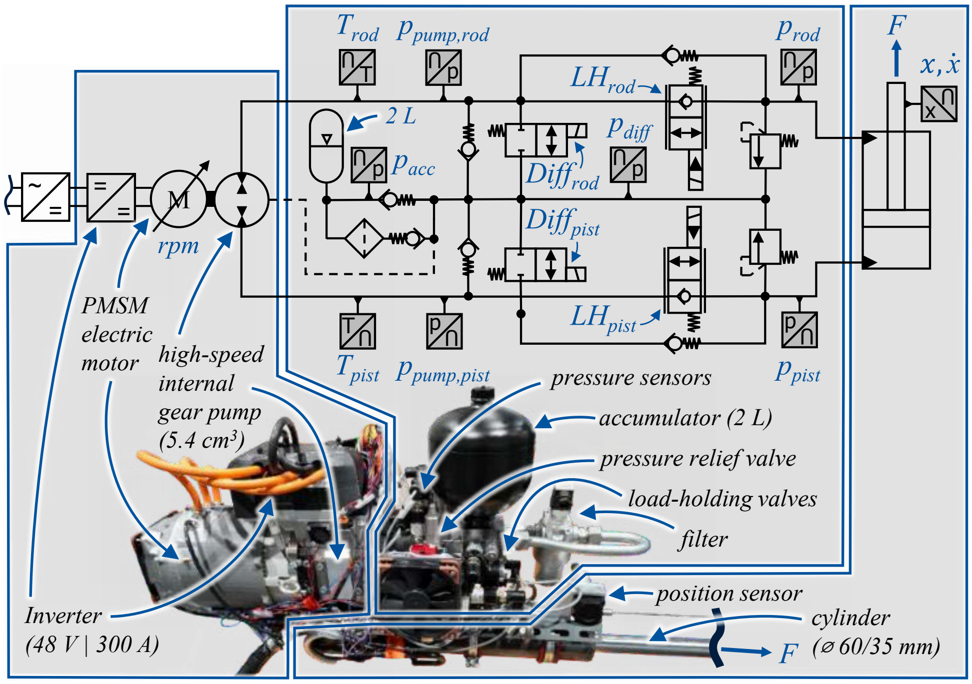

Figure 2.1. Circuit layout and functional model of the high-speed EHA

a dig and dump cycle on a 1.8-ton excavator's arm is around 4 kW. Consequently, software limits the motor's output to 6 kW to account for power losses. The hydraulic unit features an internal gear design with a displacement volume of 5.4 cm³ and is optimized for operation up to 10,000 rpm. The pump is flange-mounted to the valve block, compactly interconnecting it with the valves, sensors, and accumulator hydraulically. Additionally, check valves parallel to the load-holding valves prevent cavitation in the cylinder while another pair near the filter and accumulator directs flow through the filter.

To achieve high rotational speeds without cavitation, a minimum absolute inlet pressure of 1.2 bar is required at the pump. The accumulator serves two functions: it stores the cylinder's differential volume (0.358 L) and maintains this minimum pressure. However, the pump shaft seal limits the maximum pressure to 10 bar. To operate within a temperature range of -10°C to +60°C, the accumulator needs a nominal volume of 2 L, achievable only if check valves between the accumulator and pump inlet have minimal pressure drop. Higher pressure drops reduce the effective pressure difference, necessitating a larger accumulator volume for storage. Therefore, check valves are installed parallel to the load-holding valves to minimize pressure drop, allowing for a lower minimum accumulator pressure and increasing the maximum pressure difference, which reduces the required nominal volume.

2.2. Control scheme

The control scheme is presented and evaluated using simulations in [9]. The most important features are summarised briefly below.

The operating boundaries, which are shown in Figure 2.2, are based on cylinder friction ($p_{bound,fric}$), accumulator pressure ($p_{bound,acc}$), and the pressure drop over the load holding valve ($p_{bound,valve}$) due to the circuit layout. The latter is problematic during motor operation due to the minimum pressure required for a given flow rate. High velocities cannot be achieved under low loads. However, since mobile machinery is used under a wide range of operating conditions that cannot be predicted in advance, an inoperative load-velocity combination is unacceptable. Therefore, the load pressure operating range of pump operation (Q1 and Q3) is expanded by actively throttling the cylinder outflow using proportional valves, in a manner comparable to metering-out systems. This enables displacement control in regions where valve losses would otherwise limit it. The aim is to maintain a fixed pressure difference over the load-holding valves using a characteristic field in combination with a PI controller. By engaging this only in regions close to the boundary, the influence on efficiency is minimized.

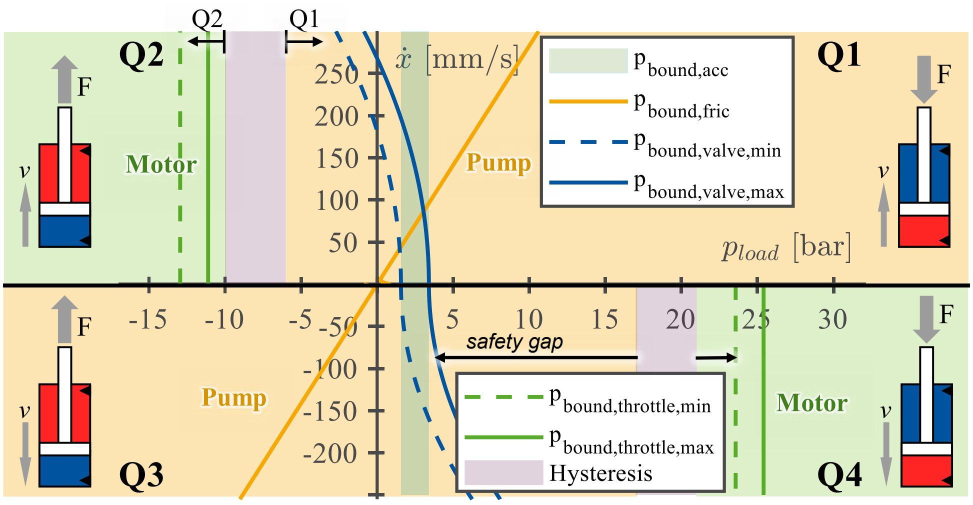

Figure 2.2. Quadrant definition used by the new control approach

However, switching from displacement to valve control still occurs at higher loads. This is denoted as the throttle boundary ($p_{bound,throttle}$) in Figure 2.2, where the 'min' and 'max' indices indicate dependency on the corresponding accumulator pressure limits. If the load pressure exceeds the current limit, the constant pressure difference request of the load-holding valves will cause the cylinder to accelerate. Therefore, switching to motor operation beforehand is necessary. Active hysteresis, marked in violet in Figure 2.2, is used to determine when the quadrant switch must be executed. During cylinder extension, mode Q1 is selected if the load pressure is above -10 bar. If the load pressure falls below this threshold, the system switches to mode Q2. Switching back to mode Q1 requires an increase in load pressure exceeding -6 bar. The positioning and width of the hysteresis band depend on the specific application and the optimization of performance. The configuration shown is for an excavator arm. Therefore, the hysteresis band is placed closer to the throttle boundary because the centre of mass generally does not cross top dead centre. This means that switches Q1→Q2 or Q3→Q4 generally do not occur. This placement enables operation under all working conditions and maximizes the safety gap, corresponding to the time between reaching a hysteresis edge and its corresponding boundary, during switches from Q2→Q1 and Q4→Q3. Thereby allowing more time for adjustment of valve positions.

The control scheme features two state machines. One determines the current operation quadrant based on the quadrant definition with active hysteresis, as shown in Figure 2.2. The other synchronizes motor speed and valve positions during quadrant switches. The hydraulic unit's volumetric efficiency, pressure feedback, and valve controllers are implemented to enable the different required valve modes, as well as to provide overload protection for the electric motor. A more detailed description is given in [9]. As described there, the control scheme used in this paper was improved to also allow for smooth transitions Q1↔Q3 with recuperation and improved pre-pressurization before motor operation.

3. EXPERIMENTAL VALIDATION

Experimental validation is performed using a hardware-in-the-loop test rig. The tests include synthetic test cases that focus on the quadrant switches, as well as different load cycles that validate the application's performance in excavators. Additionally, a quadrant-based efficiency map and the efficiencies under different load cycles are calculated.

3.1. Hardware-in-the-loop test rig

The hardware-in-the-loop (HiL) test rig, introduced in [23], primarily consists of two load cylinders and associated servovalves, as shown in Figure 3.1. The load cylinder rods are mechanically linked to the EHA cylinder rod via a movable crossbeam, enabling the application of pulling or pushing forces. The actual force on the EHA differs from the hydraulic force due to friction, which is measured by a load cell. While the friction forces from the load cylinders increase system damping compared to excavator applications and the moving mass of the Hil of roughly 100 kg is lower than that of an excavator arm, the HiL setup allows for repeatable and adjustable testing conditions for the EHA.

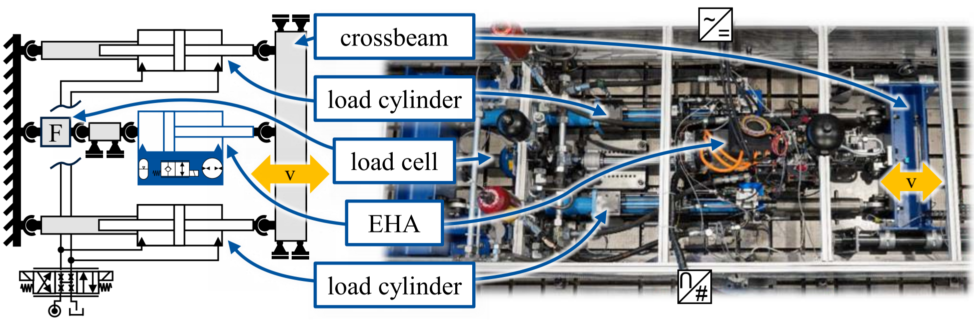

Figure 3.1. Hardware-in-the-loop (HiL) test rig (simplified hydraulic circuit layout)

Although controlling the HiL test rig is not the focus of this paper, a few important notes are provided below. The system is rather stiff due to the hydraulic tension between the load cylinders and the EHA, which complicates force control. Small errors in the flow rate of the valve-controlled cylinders result in significant force changes due to the system's high stiffness, which is caused by the bulk modulus of the oil. To achieve acceptable force control, it is necessary to predict the cylinder flow rate, and thus, cylinder velocity, to enable feed-forward control of the rough valve position. A PID controller then fine-tunes the position to achieve good force accuracy. However, for feed-forward control, simply calculating velocity by differentiating the position signal introduces lag due to the required filtering. This lag results in temporary, large differences between the required and actual valve positions, leading to significant force deviations. Therefore, an approach is necessary that predicts cylinder movement based on pump speed and valve actuation. Valve actuation must be considered separately due to temporary switching to valve control of cylinder speed, for example, when stopping. A perfect prediction still was not achieved.

3.2. Synthetic test cases

The synthetic test cases examined are depicted in Figure 3.2 and are identical to those previously analyzed through simulations. The first test case is called ‘velocity reversal’, representing quadrant switches by reversing the direction of movement under constant load force F. The second test case entails a force reversal, which linearly alters the load force during movement at a constant velocity. Here, F_{mean} represents the midpoint of the hysteresis band, and ΔF is half the change in force over a duration of 0.5 seconds.

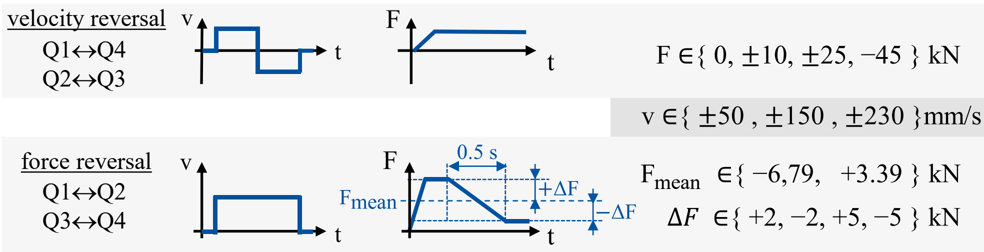

Figure 3.2. Synthetic test cases

3.3. Load cycles

The authors had access only to a measured dig and dump load cycle of a 1.8-ton excavator. To evaluate the EHA under a broader range of working conditions, load cycles from the STEAM research project were scaled to fit within operational limits:

1. The load pressure profile is scaled to not exceed the maximum operational pressure.
2. The cylinder position is filtered and differentiated to obtain the velocity profile, which is then scaled to remain within the maximum operational velocity.
3. By integrating the scaled velocity profile, a new cylinder stroke profile is generated.
4. If the cylinder end stops are reached, the time is adjusted to reduce the duration of EHA movement, thereby decreasing the maximum stroke.

It is important to note that this approach modifies not only the absolute values of the profiles but also their gradients. However, these profiles remain related to the measured data, and such alterations appear acceptable given that profiles can vary significantly between different machines as well as depending on current work conditions and operator actions.

4. RESULTS & DISCUSSION

The cylinder velocity in the following results is calculated by filtering the measured position signal. A significant challenge in evaluating performance is achieving operator acceptance during EHA operation, which is inherently subjective. The authors were unable to identify a meaningful method to assess this type of acceptance for mobile machinery and strongly recommend that it be evaluated separately. Consequently, the performance rating in this paper is based on the calculated velocity and the authors' considerations.

4.1. Test cases

Figure 4.1 displays the results of the velocity reversal test case. The results are divided into six subgroups based on the initial velocity. The top graph in each group displays the cylinder velocity, and the bottom graph shows the calculated hydraulic force based on the load pressure and the cylinder piston area. Positive force values represent a pulling force at the cylinder.

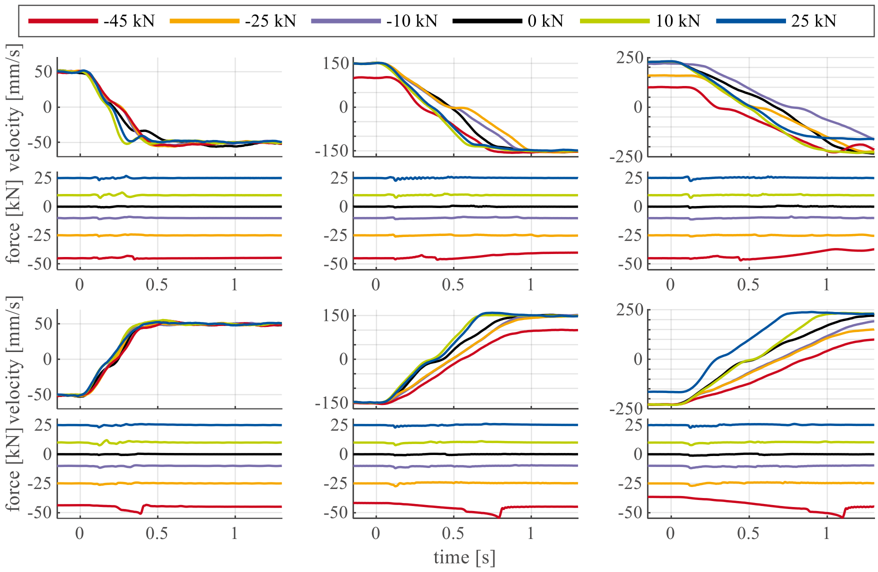

Figure 4.1. Experimental results for test case 'velocity reversal' (force based on p_{load})

As intended, the forces during the reversal are constant, except for the -45 kN case, which shows smaller deviations. As can be seen from the velocities, high velocity and load combinations result in a power limitation of the motor and, therefore, a smaller-than-requested cylinder velocity. Negative forces correlate with a loaded piston side, requiring higher flow rates and rotational speeds. Therefore, the torque capacity of the electric motor is reduced further, resulting in slower acceleration and deceleration. The top group of graphs represents positive initial velocities. As expected, a linear velocity change is achieved for positive pulling forces (Q2→Q3) and zero load (Q1→Q3). For negative forces (Q1→Q4), the designed rest phase, which allows time for LH_{rod}, $Diff_{rod}$, and LH_{pist} to open and close, respectively, can be seen at about zero velocity.
The bottom group represents negative initial velocities. For these, a negative pushing force (Q4→Q1) results in a linear velocity change. Positive forces (Q3→Q2) and no load (Q3→Q1) demonstrate the intended rest state, allowing time for LH_{pist} to open and LH_{rod} and $Diff_{rod}$ to close.

In conclusion, the velocity reversal test cases show the desired and expected behaviour. The velocity reversal is smooth and does not show strong oscillations.

The results for the 'force reversal' test case are displayed in Figure 4.2, grouped by the corresponding quadrant switch. The graphs on the left side show results for zero load. In contrast to the velocity reversal, larger deviations from the set force (dashed black line) are

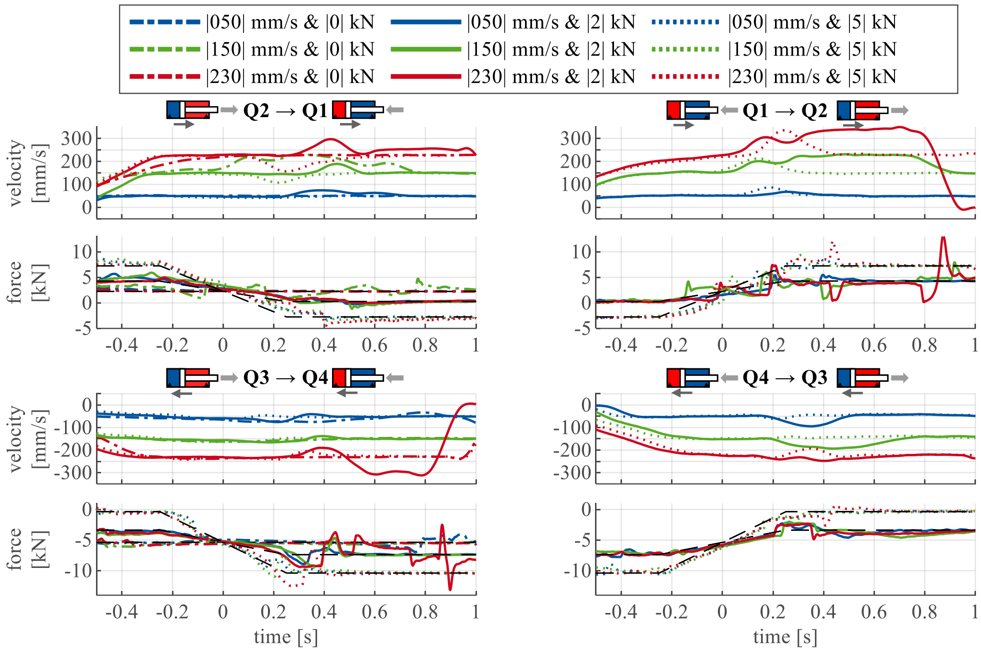

Figure 4.2. Experimental results for test case ‘force reversal’ (force based on p_{load}) (set force marked with a black dashed line)

evident in some test cases, particularly during Q1→Q2 and Q3→Q4 at high velocities. The interaction between the EHA and force control of the HiL during initial switches leads to deviations so significant that they can trigger additional switches.

As previously mentioned, force control in the HiL is challenging due to system stiffness combined with changing valve states, making it difficult to accurately identify the root cause of these deviations. However, despite these challenges, good velocity tracking is achieved when examining the velocity graphs of cases with effective force tracking.

For switches Q2→Q1, the no-load case at 150 mm/s stands out as an outlier in terms of velocity tracking, which can be attributed to mode switches resulting from poor force tracking. In contrast, the other no-load test cases demonstrate good tracking. When force changes of 2 kN occur, short and minor overshoots are observed due to the motor speed increasing while still supporting some cylinder load, coupled with the valve not being in the correct throttling position because of its dynamics. At higher change rates, the force begins to slow down the cylinder sooner, and the pump speed fails to increase quickly enough to supply the required power. Consequently, deviations increase with rising cylinder velocity due to heightened friction.

During the Q1→Q2 switches, initial overshoots are observed due to the assistive load accelerating the cylinder before displacement control is reestablished through a slowdown of the hydraulic unit. Faster force changes lead to greater deviations because of increased acceleration, while not under displacement control.

Q3→Q4 switches show small negative deviations at lower velocities and smaller load changes. This is attributed to the assistive load still being applied while the valve lags before throttling and slowing down the cylinder.

For Q4→Q3 switches, overshoots appear for small force change rates, again due to assistive load being applied and valve lagging before throttling can slow down the cylinder. The prolonged deviation at -150 mm/s with 2 kN can be traced back to an extended adjustment period of the valve position by the PI controller, likely resulting from inaccuracies in the characteristic field that necessitate longer adjustments.

The results for most cases qualitatively match the simulation results presented in [10]. Exceptions include the Q2→Q1 switches with slow change rates, which show an overshoot instead of the simulated undershoot, and the Q1→Q2 switches with slow change rates, where experimental results reveal an overshoot while simulations indicate almost no deviation. These discrepancies may stem from differences in moving mass and friction between the simulation and the hardware-in-the-loop (HiL) test rig.

In conclusion, the force reversal test cases demonstrate that quadrant switches, excluding those with problematic force application due to coupling between HiL and EHA, can be executed with only short and limited deviations in the velocity profile. Although perfect tracking is unattainable due to valve lag and rotational speed adjustments, it has been demonstrated that the developed control scheme can effectively mitigate the severity of these issues.

4.2. Efficiency map

Figure 4.3 shows the efficiency map of the EHA, which was calculated based on measurements taken under quasi-stationary conditions. The cylinder is loaded, accelerated, and stopped again. Due to the limited cylinder stroke, the 400 ms period before deceleration is evaluated. The efficiency is interpolated between the marked measurement points, resulting in anomalies at the outer edges of the efficiency field due to the algorithm used. Additionally, reduced motor performance is evident at higher speeds in Q1, Q3, and Q4. Efficiency is calculated using Equation 4.2, which considers mechanical (Equation 4.3), electrical (Equation 4.4), and hydraulic energy from the accumulator (Equation 4.5). Therefore, all system losses, including those of the inverter, electric motor and cylinder, but excluding those of the valve actuation, are considered. Depending on the sign of the total transferred energy, the different parts are considered output or input in Equation 4.2.

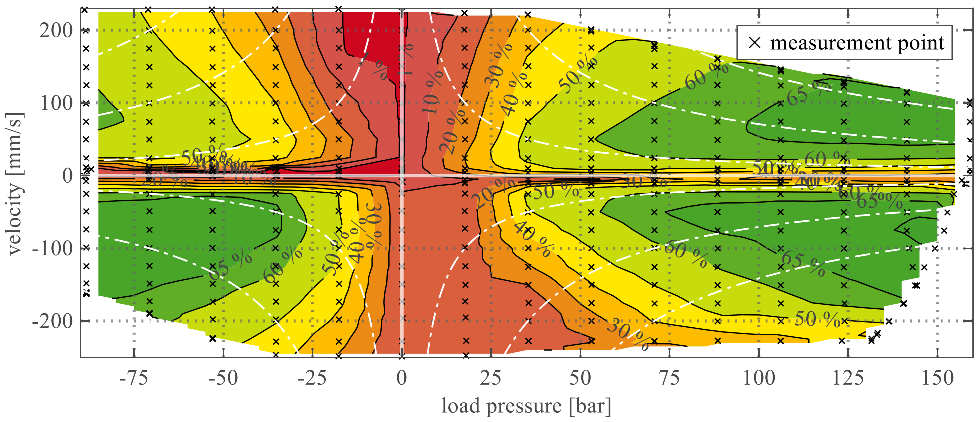

Figure 4.3. Efficiency map of the EHA (isolines for cylinder power neglecting friction of 0.5, 2 & 4 kW)

$$\eta = \frac{E_{out}}{E_{in}} \tag{4.2}$$

$$E_{mech} = \int F_{cyl} \cdot v_{cyl}\, dt \tag{4.3}$$

$$E_{elec,powersupply} = \int U_{sup} \cdot I_{sup}\, dt \tag{4.4}$$

$$E_{acc} = \int Q_{acc} \cdot p_{acc}\, dt \quad \text{with} \quad Q_{acc} = (A_{pist} - A_{rod}) \cdot v_{cyl} \tag{4.5}$$

Except for Q2, the highest efficiencies per quadrant exceed 65% for moderate velocities and high loads. The added isolines for cylinder power outputs of 0.5 kW, 2 kW, and 4 kW indicate that areas with poor efficiency correlate with low power transfer, resulting in minimal absolute power loss. The regions of low efficiency at low loads in Q2 and Q4 correspond to the expanded areas in Q1 and Q3, where a significant portion of energy input is lost due to active throttling. In Q2 at high velocities, there is no power output from the cylinder due to friction; instead, all power input from the pump and accumulator is converted to heat. In contrast, Q4 exhibits higher efficiency because the accumulator is charged.

The impact of load-holding valve losses, along with cylinder and pump friction at higher speeds, is evident. The pressure difference across the load-holding valves is particularly relevant in Q1 and Q3, as it remains constant, leading to linear increases in losses with increasing cylinder velocity. Interestingly, efficiencies in Q1 and Q4 are comparable; however, this is not the case for Q2 and Q3. This discrepancy most likely arises from the interplay between the hydraulic unit's efficiency and the efficiency of energy storage in the accumulator. In Q2, these effects negatively combine, while in Q4, the higher efficiency of energy storage counteracts the lower motor operation efficiency.

4.3. Load cycles

Figure 4.4 shows the results of the 1.8-t dig and dump cycle. The results are limited to the first 13 seconds to allow for a higher level of detail. A simple outer PI controller was added to adjust the requested speed, which was calculated offline beforehand, based on the deviation between the requested and current position during the tests. These values, as well as accumulator pressure, are shown in graph 1 (see grey box in Figure 4.4). A maximum RMSE of 75.45 mm and an ITAE of 34 ms^2 are achieved over the 55 second cycle. The deviations can be traced back to the cylinder velocities shown in graph 5. There is a delay between the request and the actual velocity. Examining the deviation between the cylinder velocity based on the actual pump speed, neglecting volumetric efficiencies (f(rpm)), and the current cylinder velocity, it can be concluded that the displacement control is functioning as intended. However, especially during deceleration phases, which are not subject to delays by the control scheme, a delay of up to 200 ms can be observed between the cylinder speed request and the rotational speed adjustment. Approximately 50 ms of this delay is related to the time between the speed request and the motor's rotational speed adjustment.

Graph 2 illustrates the pressures in the cylinder chamber and the hydraulic unit ports. Following each entry into a quadrant (as shown in Graph 3), higher pressure levels are initially observed due to the delayed adjustment of the load-holding valve position. This phenomenon is further evidenced in graph 4, which displays the adjustment of current over

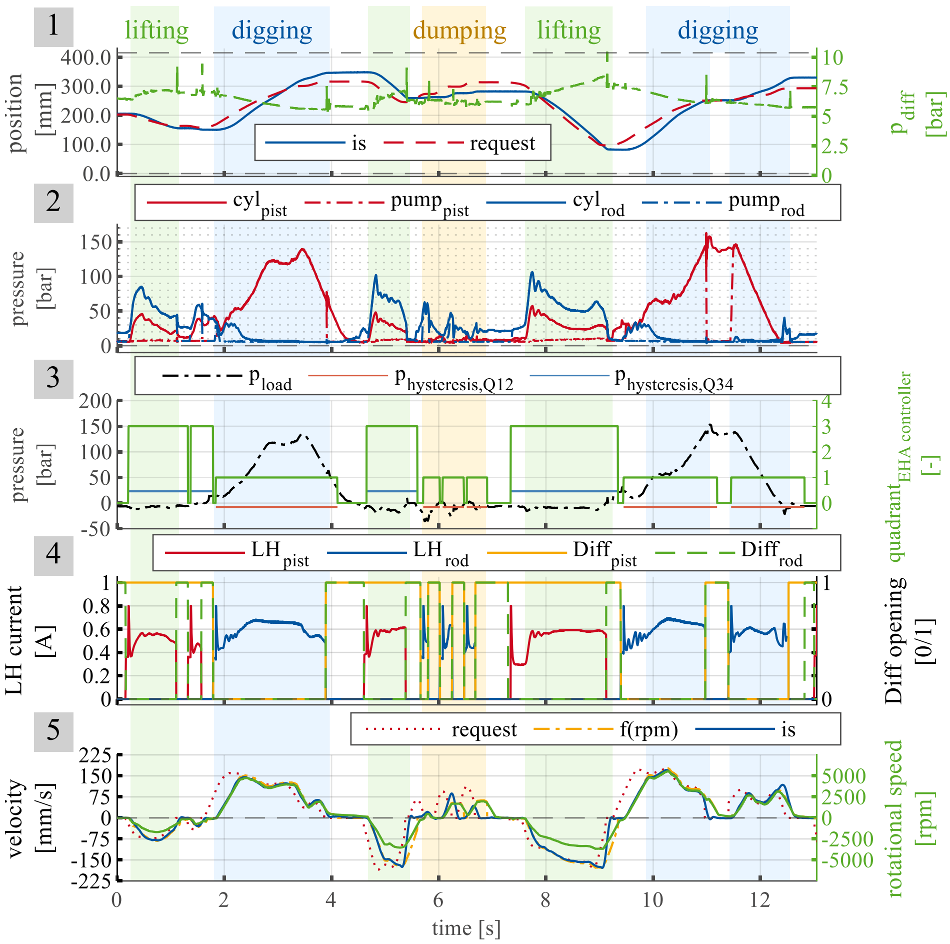

Figure 4.4. Experimental results of the 1.8-t excavator dig and dump cycle with outer position controller

time alongside the actuation signal of the differential valves. The initial peak in the actuation signal for the load-holding valves at maximum current is designed to open the valve promptly, preventing hydraulic tensioning of the cylinder caused by obstructed outflow.

Shortly after 6 seconds and again at 12 seconds, peaks in the cylinder velocity request are observed. At these moments, the cylinder speed exceeds that based on pump speed, indicating a loss of displacement control. During these instances, the load pressure drops below the hysteresis band between Q1 and Q2, as shown in Graph 3. This triggers a mode switch towards the motoring quadrant (Q1→Q2), which is associated with an overshoot, as previously illustrated in Figure 4.2.

It is important to note that the load cycle was measured in a valve-controlled system. The measured load is applied based on time without feedback from the cylinder position. Consequently, some working conditions may differ when implemented on a real excavator due to changes in system response. Nevertheless, the overall tracking of the reference load cycle is achieved, albeit with some deviations primarily attributed to initial delays inherent in the control scheme and partially due to delays in the motor response.

The authors acknowledge their lack of a meaningful metric for assessing performance in the context of mobile machinery. A review of existing research on teleoperation, as referenced in [24], indicates that latencies below 250 ms or 300 ms are acceptable, with less than 170 ms being preferable for autonomous vehicles. Ideally, the time between input and output should be under 80 ms. While direct transfer may not be entirely suitable, the delays experienced by the EHA generally fall within an acceptable latency range; however, input-output delays occasionally exceed this threshold.
Given that operators can adjust for these delays, the successful application of this technology in an excavator appears feasible. Nonetheless, further testing with real human operators in an excavator is necessary and recommended to gather subjective feedback.

The efficiency of the developed EHA is evaluated based on the available load cycles. The energy transfers considered include electrical energy from the DC side of the power supply, hydraulic energy from the accumulator, and mechanical energy from the cylinder. Energy transfer is aggregated for input and output per system boundary by calculating power transfer at each sample point, multiplying it by the time difference between samples, and then summing all negative and positive values separately (eq. (4.3)-(4.5)). Since operation during the cycles is not quasi-stationary, the flow rate is estimated based on current quadrant operation and valve actuation, which introduces some inaccuracies due to partially open valves and volume changes resulting from compression.

As discussed in [11], there is currently no consensus on how to calculate the efficiency of systems with recuperation capability. Therefore, Table 4.1 presents three different definitions based on the experimental results from the adjusted STEAM load cycles, along with the calculated energy transfers and total energy loss. The very limited bucket movement during air grading leads to questionable efficiency results.

Table 4.1. Transferred energies (negative values exiting the system), efficiencies and dissipation ratios for the adjusted 18-t STEAM load cycles per actuator

	Dig and dump			**Air grading**			**Excavating**		
	boom	arm	bucket	boom	arm	bucket	boom	arm	bucket
$E_{cyl,out}$ [kJ]	-144.3	-24.9	-50.5	-55.0	-0.7	-0.04	-69.2	-41.1	-34.3
$E_{cyl,in}$ [kJ]	113.8	21.5	9.5	48.6	7.6	0.26	65.1	4.5	10.0
$E_{elec,in}$ [kJ]	237.2	122.5	168.0	88.9	51.2	0.66	127.0	129.5	115.0
$E_{elec,out}$ [kJ]	-53.9	-21.3	-7.7	-30.2	-7.9	-0.08	-39.3	-10.1	-6.3
$\sum E_{acc}$ [kJ]	-0.88	-2.04	-0.75	-0.06	-0.88	-0.05	-0.50	-0.38	-0.66
E_{loss} [kJ]	151.8	95.7	118.5	52.3	49.3	0.75	83.2	82.3	83.8
$\eta_1 = \frac{\lvert E_{cyl,out}\rvert}{\sum E_{elec} + \sum E_{acc}}$	79.1 %	25.1 %	31.6 %	93.7 %	1.6 %	*8.1 %*	79.3 %	34.5 %	31.7 %
$\eta_2 = 1 - \frac{E_{loss}}{E_{elec,in} + E_{acc,in} + E_{cyl,in}}$	57.1 %	33.9 %	34.2 %	62.3 %	16.6 %	*19.3 %*	57.1 %	39.3 %	33.9 %
$DR = \frac{E_{loss}}{\lvert E_{cyl,out}\rvert + \lvert E_{cyl,in}\rvert}$	0.59	2.06	1.98	0.50	5.98	*2.48*	0.62	1.81	1.89

The first definition, η_1, considers only the positive cylinder output in relation to the total energy input. The second definition, η_2, incorporates the energy input of the cylinder by relating energy loss to the sum of positive energy inputs. Lastly, a new key performance indicator, termed ‘dissipation ratio’ (DR), is introduced as the ratio of power loss to the absolute value of transferred cylinder energy [10]. The dissipation ratio effectively addresses issues associated with the cancellation of energy transfers in other definitions, which can result in negative or misleading efficiency values. It is important to note that smaller dissipation ratio values indicate higher efficiency due to reduced energy loss, while ratios exceeding one may also occur.

The results clearly indicate that the highest efficiencies, regardless of the definition used or the load cycle analyzed, are achieved for the excavator boom. The boom also exhibits the highest energy inputs from the cylinder for all load cycles, likely due to the supported mass consisting of the boom, arm, and bucket. The substantial energy inputs correspond with high electric energy outputs. However, this very electric energy output is responsible for the previously mentioned cancellation in the denominator of efficiency definition one, which can theoretically lead to an efficiency value exceeding one.

Table 4.2 presents the efficiency η_2 and dissipation ratio (DR) results for various linear scalings of the velocity and load of the 1.8-ton dig and dump cycle. For both definitions, efficiency increases with higher loads, as smaller DR values correspond to higher efficiency. This trend aligns with the efficiency map shown in Figure 4.3, which indicates that efficiency improves with increasing loads. Conversely, a decrease in efficiency is typically expected at higher velocities; however, η_2 shows an increase instead. This phenomenon occurs because energy is stored in the drive train's inertia during acceleration, resulting in a higher electric energy input (denominator). During deceleration, this energy is converted back into electric output (numerator), resulting in a shift toward higher ratios. This highlights a misleading result that can arise from current efficiency definitions. In contrast, the dissipation ratio behaves as expected, decreasing with greater loads and increasing with higher velocities, except for a minor decrease at higher loads and lowest velocities, which might be the result of higher friction at lower speeds as well. Thereby validating its role as an appropriate key performance indicator for systems with recuperation capability.

Table 4.2. Efficiency and dissipation ratios for the scaled 1.8-t dig and dump cycle

	$\eta_2 = 1 - \frac{E_{loss}}{E_{elec,in} + E_{acc,in} + E_{cyl,in}}$				$DR = \frac{E_{loss}}{\lvert E_{cyl,out}\rvert + \lvert E_{cyl,in}\rvert}$			
	25 % F	50 % F	75 % F	100 % F	25 % F	50 % F	75%	100 % F
25 % v	14.7%	24.1%	32.1%	37.6%	6.893	3.252	2.090	1.609
50 % v	16.4%	26.5%	34.3%	40.3%	7.385	3.197	2.009	1.526
75 % v	17.6%	27.0%	34.3%	41.0%	8.499	3.440	2.152	1.556
100 % v	18.4%	27.9%	34.9%	41.0%	8.880	3.550	2.215	1.612

5. CONCLUSION & OUTLOOK

This study presents a newly developed EHA that incorporates a high-speed internal gear unit and a differential cylinder, enabling recuperation and load-holding capabilities. The EHA was experimentally tested in a hardware-in-the-loop test rig and specifically sized for use in an 1.8-ton excavator. The design focuses on a novel control approach that aims to minimize velocity deviations during quadrant switches through active throttling and active hysteresis.

Performance validation during quadrant switches was achieved using specially designed test cases. Under varying loads, the actuator demonstrated smooth cylinder velocity without oscillations when changing direction of movement. When the load direction changed during a constant velocity request, corresponding to an operational quadrant shift, only short and limited velocity deviations occurred, despite adjustments to valve positions and motor speed.

The tracking of a measured dig and dump cycle for the 1.8-ton excavator is sufficnet for use in excavators, although some deviations between the requested and actual positions were noted due to delays inherent in the control scheme. The efficiency of the EHA under tested working conditions reached 65% in three of the four quadrants, with an overall maximum efficiency of 70%. Analysis based on three downscaled load cycles (dig and dump, air grading and excavating) for an 18-ton excavator load cycles concluded that the highest efficiency, regardless of load cycle or energy efficiency definition, was achieved by the boom actuator.

Additionally, it was highlighted that current efficiency definitions often neglect energy stored in the drive train, resulting in misleading results. In contrast, a new key performance indicator introduced by the authors, termed ‘dissipation ratio’, more accurately reflects true system performance.

This contribution shows the high potential of the new EHA design and control approach. Future works include the implementation of the EHA on a real excavator to assess operator acceptance, address challenges related to force control in hardware-in-the-loop testing, and evaluate the interaction between excavator kinematics and the EHA.

6. ACKNOWLEDMENT

The IGF research project ‘22246 N / 1’ of the research association Forschungskuratorium Maschinenbau e. V. – FKM, Lyoner Straße 18, 60528 Frankfurt am Main was supported from the budget of the Federal Ministry of Economic Affairs and Climate Action through the DLR within the scope of a program to support industrial community research and development (IGF) based on a decision of the German Bundestag.

7. REFERENCES

[1] Love, L. J., Lanke, E., Alles, P. 'Estimating the Impact (Energy, Emissions and Economics) of the U.S. Fluid Power Industry - Tech. Rep. ORNL/TM-2011/14.', 2012.

[2] Zimmerman, J. D., Pelosi, M. et al. 'Energy Consumption of an LS Excavator Hydraulic System', Volume 4: Design, Analysis, Control and Diagnosis of Fluid Power Systems, pp. 117–126, 2007. DOI: 10.1115/IMECE2007-42267.

[3] Gøytil, P. H., Padovani, D., Hansen, M. R. 'On the Energy Efficiency of Dual Prime Mover Pump-Controlled Hydraulic Cylinders', ASME/BATH 2019 Symposium on Fluid Power and Motion Control, 2019. DOI: 10.1115/FPMC2019-1642.

[4] Pietrzyk, T., Schmitz, K. 'Messtechnische Erprobung einer elektro-hydraulischen Linearachse mit High-Speed Antrieb', Hybride und energieeffiziente Antriebe für mobile Arbeitsmaschinen: 8. Fachtagung, 23. Februar 2021, Karlsruhe.

[5] Pietrzyk, T., Schmitz, K. et al. 'Entwicklung und Auslegung einer elektro-hydraulischen Achse mit einem 48 V High-Speed-Antrieb zur Dezentralisierung der Arbeitshydraulik eines Kompaktbaggers', Hybride und energieeffiziente Antriebe für mobile Arbeitsmaschinen: 7. Fachtagung, 20. Februar 2019, Karlsruhe.

[6] Pietrzyk, T., Roth, D. et al. 'Design of a High Speed Internal Gear Pump to Increase the Power Density of Electro Hydraulic Actuators (EHA) in Mobile Applications', Volume 7: Fluids Engineering, 2019. DOI: 10.1115/IMECE2019-10351.

[7] Pietrzyk, T., Roth, D. et al. 'Design study of a high speed power unit for electro hydraulic actuators (EHA) in mobile applications', 11th International Fluid Power Conference, 2018. DOI: 10.18154/RWTH-2018-224632.

[8] Pietrzyk, T. 'Entwicklung einer Hochdrehzahl-Innenzahnradpumpe für die Elektrifizierung mobiler Anwendungen am Beispiel einer autarken dezentralen elektro-hydraulischen Achse', 2022. DOI: 10.18154/RWTH-2022-00767.

[9] Figge, F., Schmitz, K. 'Simulative controller evaluation for an electro-hydrostatic excavator actuator with load-holding capability using active hysteresis and throttling control', The 19th Scandinavian International Conference on Fluid Power, SICFP'25, 2025.

[10] Figge, F., Schmitz, K. 'EHAs in mobile machinery: Simulative evaluation of a control scheme including load-holding capability using active hysteresis and throttle control', International Journal of Fluid Power, accepted for publication on 18 December 2025.

[11] Figge, F., Reinertz, O., Schmitz, K. 'Review of efficiency definitions for systems with energy recuperation and introduction of the dissipation ratio', Proceedings of the ASME 2025 International Design Engineering Technical Conferences and Computers and Information in Engineering Conference, 2025.

[12] Figge, F., Schmitz, K. 'Simulative Comparison Approach of Electro-Hydrostatic Actuator Circuits in Excavators', ASME/BATH 2023 Symposium on Fluid Power and Motion Control, 2023. DOI: 10.1115/FPMC2023-111798.

[13] Williamson, C., Ivantysynova, M. 'Stability and motion control of inertial loads with displacement controlled hydraulic actuators', 6th FPNI-PhD Symp, pp. 499–514, 2010.

[14] Michel, S. 'Elektrisch-hydrostatische Kompaktantriebe mit Differentialzylinder für die industrielle Anwendung', Dissertation, Dresden, 2020. DOI: 10.25368/2021.86.

[15] Williamson, C., Ivantysynova, M. 'Pump mode prediction for four-quadrant velocity control of valveless hydraulic actuators', 7th JFPS International Symposium on Fluid Power, 2008.

[16] Wang, L., Book, W. J., Huggins, J. D. 'A Hydraulic Circuit for Single Rod Cylinders', Journal of Dynamic Systems, Measurement, and Control, Vol. 134, Nr. 1, 2012. DOI: 10.1115/1.4004777.

[17] Çalışkan, H., Balkan, T., Platin, B. E. 'A Complete Analysis and a Novel Solution for Instability in Pump Controlled Asymmetric Actuators', Journal of Dynamic Systems, Measurement, and Control, Vol. 137, Nr. 9, 2015. DOI: 10.1115/1.4030544.

[18] Imam, A., Rafiq, M. et al. 'Design, Implementation and Evaluation of a Pump-Controlled Circuit for Single Rod Actuators', Actuators, Vol. 6, Nr. 1, pp. 10, 2017. DOI: 10.3390/act6010010.

[19] Imam, A., Tolba, M. S., Sepehri, N. 'Improving performance of pump-controlled hydraulic circuits for single-rod actuators: conceptual study', Journal of Physics: Conference Series, Vol. 2616, Nr. 1, pp. 12015, 2023. DOI: 10.1088/1742-6596/2616/1/012015.

[20] Koury Costa, G., Sepehri, N. 'A Critical Analysis of Valve-Compensated Hydrostatic Actuators: Qualitative Investigation', Actuators, Vol. 8, Nr. 3, pp. 59, 2019. DOI: 10.3390/act8030059.

[21] Gøytil, P. H., Padovani, D., Hansen, M. R. 'A Novel Solution for the Elimination of Mode Switching in Pump-Controlled Single-Rod Cylinders', Actuators, Vol. 9, Nr. 1, pp. 20, 2020. DOI: 10.3390/act9010020.

[22] Kärnell, S., Ericson, L. 'Hysteresis Control in Pump-Controlled Systems—A Way to Reduce Mode-Switch Oscillations in Closed and Open Circuits', Energies, Vol. 15, Nr. 2, pp. 424, 2022. DOI: 10.3390/en15020424.

[23] Haas, C., Schmitz, K. 'Control Strategy for a Hardware in the Loop Test Bench', Advances in Hydraulic and Pneumatic Drives and Control 2023, 2024. DOI: 10.1007/978-3-031-43002-2_9.

[24] Kamtam, S. B., Lu, Q. et al. 'Network Latency in Teleoperation of Connected and Autonomous Vehicles: A Review of Trends, Challenges, and Mitigation Strategies', Sensors (Basel, Switzerland), Vol. 24, Nr. 12, 2024. DOI: 10.3390/s24123957.

Biographies

Felix Figge received the bachelor's degree in mechanical engineering with a specialization in design methodology in 2019 and the master's degree in mechanical engineering with a specialization in product development in 2021, both from RWTH Aachen University. He is currently working as a Research Associate at the Institute for Fluid Power Drives and Systems (ifas), RWTH Aachen University. His research encompasses fluid power systems in general but focuses on the development of an electro-hydrostatic actuator for use in mobile machinery.

Prof. Katharina Schmitz studied mechanical and chemical engineering at RWTH Aachen University and Carnegie Mellon University, Pittsburgh (USA) and graduated in 2015 as Dr.-Ing. at RWTH Aachen University. Since 2018, she is full professor at RWTH Aachen University and director of the Institute for Fluid Power Drives and Systems (ifas). In addition, she is Vice Dean of the Faculty for Mechanical Engineering at RWTH Aachen, a position she holds since 2020. Prof. Schmitz’s awards and honors include several best paper awards and 2023 IMechE Joseph Bramah Medal award.